# The GEO-SEQ Project
# Quarterly Status and Cost Report
# **June 1, 2001 – August 31, 2001**

## Project Overview:

The purpose of the GEO-SEQ project is to establish a public-private R&D partnership that will:

- Lower the cost of geologic sequestration by
  (1) Developing innovative optimization methods for sequestration technologies with collateral economic benefits (such as enhanced oil recovery (EOR), enhanced gas recovery (EGR), and enhanced coalbed methane production)
  (2) Understanding and optimizing trade-offs between $CO_2$ separation and capture costs, compression and transportation costs, and geologic sequestration alternatives.

- Lower the risk of geologic sequestration by
  (1) Providing the information needed to select sites for safe and effective sequestration
  (2) Increasing confidence in the effectiveness and safety of sequestration through identifying and demonstrating cost-effective monitoring technologies
  (3) Improving performance-assessment methods to predict and verify that long-term sequestration practices are safe, effective, and do not introduce any unintended environmental effects.

- Decrease the time to implementation of geologic sequestration by
  (1) Pursuing early opportunities for pilot tests with our private sector partners
  (2) Gaining public acceptance.

Technical work began in May 2000 with an initial focus on four tasks: (A) development of sequestration co-optimization methods for EOR, depleted gas reservoirs, and brine formations; (B) evaluation and demonstration of monitoring technologies for verification, optimization, and safety; (C) enhancement and comparison of computer-simulation models for predicting, assessing, and optimizing geologic sequestration in brine, oil and gas, and coalbed methane formations; and (D) improvement of the methodology and information available for capacity assessment of sequestration sites. Work continued on these four tasks during the fifth quarter. Technical progress and accomplishments are discussed below.

## Highlights:

- Calculations suggest a number of approaches which could be used to increase $CO_2$ storage during EOR, including: optimizing water injection, maximizing $CO_2$ concentration in injection gas, optimizing injection profile, injection into underlying aquifers, and reservoir repressurization (Subtask A-1).
- Reaction-progress chemical thermodynamic calculations show that clays may be an important component in the possible suite of secondary minerals that may form during $CO_2$ injection (Subtask A-3).
- Reservoir simulation has been combined with geophysical simulation, field measurements, and data analysis to illustrate the application of crosswell seismic and electromagnetic techniques for monitoring $CO_2$ injection in the Lost Hills, California, oil field (Subtask B-1 and B2).
- Capabilities of available coal bed methane numerical simulators are being assessed through testing on a series of benchmark problems. Five codes give comparable results for baseline singe-well and 5-spot $CO_2$ injection problems (Subtask C-1).
- A site in the Houston, Texas, area was identified for a field test of $CO_2$ sequestration in a brine formation. Site-specific modeling was performed to access feasibility and scope of various in-situ experiments (Task D).

## Papers Published and Presented:

Oldenburg, C.M., and S.M. Benson, "$CO_2$ injection for enhanced gas production and carbon sequestration," paper proposal accepted at SPE International Petroleum Conference and Exhibition, Villa Hermosa Mexico, 2002.

Pruess, K., C.M. Oldenburg, G.J. Moridis, and S.W. Webb, "Vertical mixing of $CO_2$ and CH4 with gravity effects", Lawrence Berkeley National Laboratory Report LBNL-48922, and abstract submitted for Fall Meeting of American Geophysical Union.

Kovscek, A.R., "Screening criteria for CO2 storage in oil reservoirs", accepted for publication in Science and Technology.

# Task Summaries

## Task A: Develop Sequestration Co-Optimization Methods

### Subtask A-1: Co-optimization of carbon sequestration and EOR and EGR from oil reservoirs.

**Accomplishments:**

- Calculations suggest a number of approaches could be used to increase $CO_2$ storage during EOR, including: optimizing water injection, maximizing $CO_2$ concentration in injection gas, optimizing injection profiles, injection into underlying aquifers, and reservoir repressurization. Selection of a particular technique is a reservoir-specific problem.
- Consideration of screening criteria for candidate reservoirs for co-optimizing EOR and sequestration shows that water in flux and pore pressure gradlients are important in addition to storage capacity, depth, injectivity, and amount of remaining oil.

**Summary:**

The objectives of this subtask are (1) to assess the feasibility of co-optimization of $CO_2$ sequestration and EOR and (2) to develop techniques for selecting the optimum gas composition for injection. Results will lay the groundwork necessary for rapidly evaluating the performance of candidate sequestration sites as well as monitoring the performance of $CO_2$ EOR.

The initial focus has been to assess the feasibility of $CO_2$ sequestration in depleted or inactive oil reservoirs. Existing $CO_2$– EOR selection criteria have been examined in light of the need to maximize $CO_2$ storage in a reservoir. New criteria have been developed and new approaches for increasing $CO_2$ storage during EOR have been identified.

*Progress This Quarter*: A study identifying several specific approaches which could be taken to increase $CO_2$ storage while at the same time enhancing oil recovery was completed. The study concluded that reservoir heterogeneity has a major impact on selection and implementation of approaches, thus making it a reservoir-specific problem. However, numerical simulations for a specific heterogeneous reservoir suggested five approaches to increasing $CO_2$ storage:

1. Adjust injection gas composition to maximize $CO_2$ concentration while maintaining an appropriate MMP.
2. Design well completions (or consider horizontal wells) to create injection profiles that reduce the adverse effects of preferential flow of injected gas through high permeability zones.
3. Optimize water injection (timing, injection rates and WAG ratio) to minimize gas cycling and maximize gas storage.
4. Consider aquifer injection to store $CO_2$ that would flow rapidly to producing wells if reinjected in the oil zone.
5. Consider reservoir repressurization after the end of the producing life of the field.

Figure 1 illustrates the effects of well completion design on oil recovery and $CO_2$ storage. Results for two strategies were provided by compositional simulations. In the first case, the injection and production wells are completed over the entire reservoir column. In the second case, the injection well is partially completed while the production well is open over the entire reservoir column. Dashed lines represent the storage factor while solid lines are cumulative oil recovery. The partial completion scheme increases both the $CO_2$ storage capacity and the cumulative oil production by a modest amount. The results also illustrate that the key-limiting factor for both oil production and $CO_2$ is the cycling of gas due to heterogeneity.

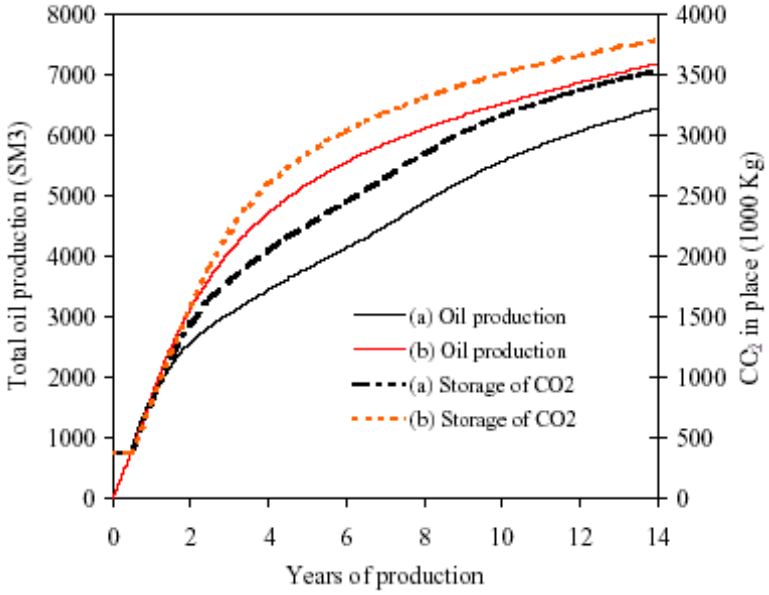


Figure 1: Compositional simulation (E300) of vertical slap geometry:
a) Injector completed over the entire reservoir column.
b) Injector completed in the three top and bottom grid blocks.

Figures 2 and 3 demonstrate the ability of WAG (water alternating gas) to increase $CO_2$ capacity of a reservoir. The figures show results from black-oil simulation of two cases with equal-sized slugs of water and $CO_2$. In the first case water and gas is injected alternating in slugs of 0.1 PV, whereas the second case uses 0.3 PV slugs. WAG injection gives better oil recovery than the waterflood and offers a reasonable emplacement of $CO_2$ into the formation. Thus, an obvious parameter to optimize is the WAG ratio, that is, the volumetric flow rate ratio of water to gas in the injected fluid. This optimization is thoroughly reservoir specific because the performance of any WAG scheme depends strongly on the distribution of permeability as well as factors that determine the impact of gravity segregation (fluid densities, viscosities and reservoir flow rates). In addition, the performance of a WAG scheme can depend strongly on the details of the flow behavior of the oil, gas and water as reflected by the two- and three-phase relative permeability. Variables that can be considered include the timing of the switch from gas to water injection, the sizes of the water and gas slugs as well as the injection rates. Further, of course, sequencing of gas, water and WAG injection across a large field can offer significant opportunities for increased gas storage.

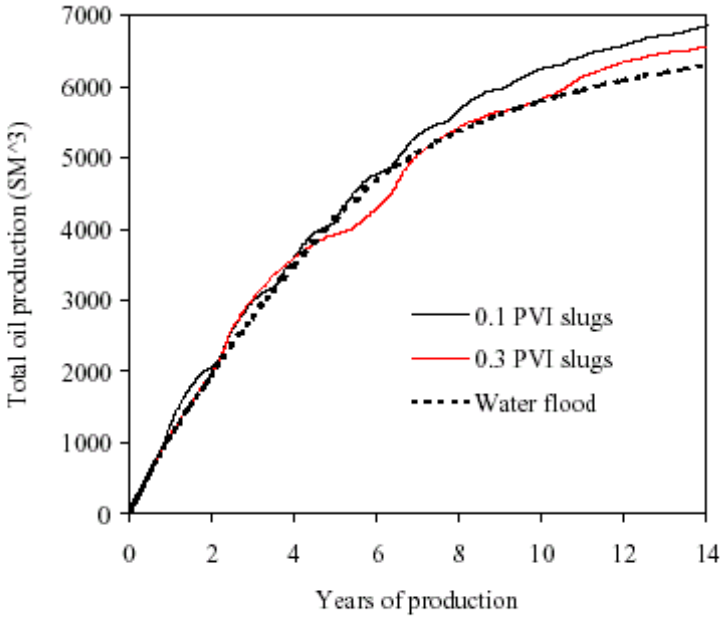


Figure 2: Oil production from waterflood and WAG schemes.

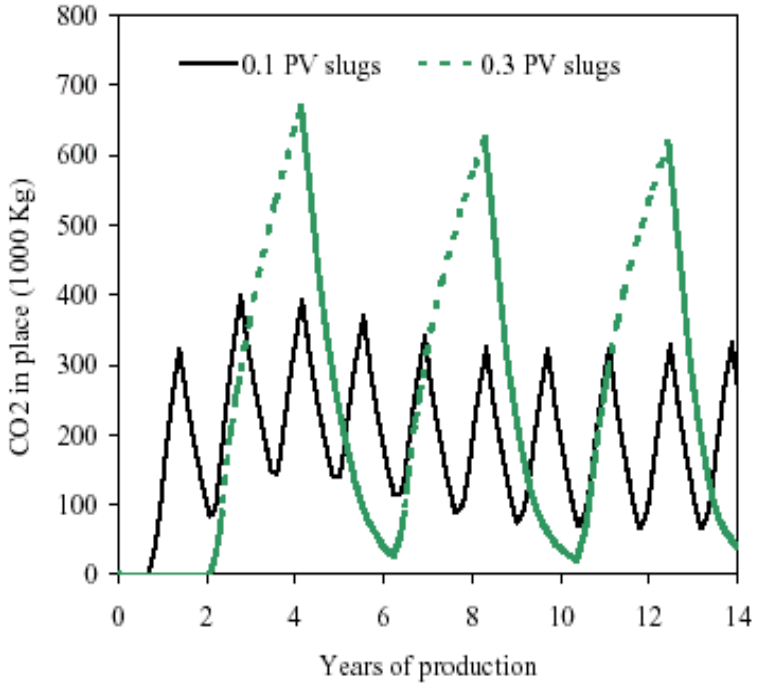


Figure 3: $CO_2$ storage capacity for WAG schemes.

The results presented above have been published in the paper "Increasing $CO_2$ Storage in Oil Recovery" by K. Jessen, L. Saur-Olibale, A. Kovscek and F. Orr.

Another paper, entitled "Screening Criteria for $CO_2$ Storage in Oil Reservoirs", authored by A. Kovscek, and submitted to the journal, Petroleum Science and Technology, presents results of study to recommend criteria for selection of oil reservoirs suitable for storage of $CO_2$ in combination with EOR a table of "Positive" and "Cautionary" factors (see September 1 – November 30, 2000 Quarterly Report) was developed for use in evaluating sites. While obvious factors include storage capacity, depth, injectivity, and amount of remaining oil, the study concludes that the density of $CO_2$ with depth alone is not a sufficient criterion for choosing candidate sites. It is also necessary to consider porosity and the amount of water and oil that displaceable. Reservoirs with weak or no water influx from underlying aquifers may be the most attractive, if all other factors are the same. In this class of reservoir, significant remaining oil might be found and reservoirs may be significantly pressure depleted. Hence, incremental oil recovery and $CO_2$ injectivity may be large. The possible integrity of reservoir seals must also be gauged. Until the time that a more complete understanding of reservoir seals is developed, it is suggested that reservoir storage sites be chosen where the initial pore pressure gradient is less than about 17.4 kPa/m. Such reservoirs are generally, effective hydrocarbon traps and should be secure sites for storage.

Finally, this quarter work began on considering aqueous surfactant-based foams in heterogeneous systems to increase $CO_2$ storage during gas injection projects. Foam should simultaneously increase oil recovery and/or be applicable to aquifer storage projects.

*Work Next Quarter*: Example reservoir simulations will begin to assess the ability of foam to increase $CO_2$ storage. In addition, application of streamline simulation to $CO_2$ sequestration will be evaluated as part of the GEOSEQ reservoir simulator intercomparison project (Task C-2).

**Subtask A-2: Feasibility assessment of carbon sequestration with enhanced gas recovery (CSEGR) in depleted gas reservoirs.**

**Accomplishments:**

- An implementation of the Dusty Gas Model for gas diffusion in porous media was tested in the TOUGH2 reservoir simulator.

**Summary:**

The objectives of this subtask are to assess the feasibility of injecting $CO_2$ into depleted natural gas reservoirs for (1) sequestering carbon and (2) enhancing methane ($CH_4$) recovery. Investigation will include assessments of (1) $CO_2$ and $CH_4$ flow and transport processes, (2) injection strategies that retard mixing, (3) novel approaches to inhibit mixing, and (4) identification of candidate sites for a pilot study.

Initial feasibility was assessed through numerical simulation of $CO_2$ injection into a model system based on the Rio Vista gas field in California. Positive results of this assessment have led to scoping studies for a CSEGR pilot. Industrial partners are now being sought.

In a parallel effort, the numerical simulation capability supporting this assessment is being improved through enhancement to the TOUGH2-EOS7C code. The first improvement was the implementation of a new real-gas-properties module, Gas Eos, which modifies gas-mixture densities and enthalpies using the Peng-Robinson equation of state.

*Progress This Quarter*: The Dusty Gas Model (DGM) for gas diffusion in porous media developed by Steve Webb at Sandia National Lab has been tested and implemented. DGM was added to TOUGH2 because it is a more accurate model for coupled gas diffusion and advection than the adjective-diffusive model (ADM) commonly used in transport simulation. In the limit of zero diffusion, the DGM and ADM are equivalent. For ordinary diffusion and Knudsen diffusion (the enhanced transport of gas components that occurs when the mean free path of gas molecules approaches the pore size), the difference between the ADM and DGM is a function of the difference in molecular weights between the gas species. For a heavy gas such as $CO_2$, these differences are expected to be important.

DGM has been implemented in the TOUGH2 $CO_2$-CH4 module EOS7C. In EOS7C, CH4 takes the place of the air component in EOS7R. Knudsen diffusion coefficients for CH4, $H_2O$, and $CO_2$ were calculated based on the Knudsen diffusion coefficient of air. Preliminary testing shows the DGM is working in

EOS7C. Simulations of gas-phase diffusion in a gravity-stable configuration were carried out using the Dusty Gas Model and the Advective Diffusive Model.

Initial simulations of the diffusive and Advective mixing of a gravity-stable CH4 of $CO_2$ gas configuration were also carried out. This configuration may be expected to exist in a depleted gas reservoir into which $CO_2$ has been injected for enhanced gas recovery and carbon sequestration. Shown in Figure 4 are profiles of the pressure and gas density at t = 0,10,50, and 100 years. This initial simulation shows only the effects of ordinary diffusion calculated with the ADM.

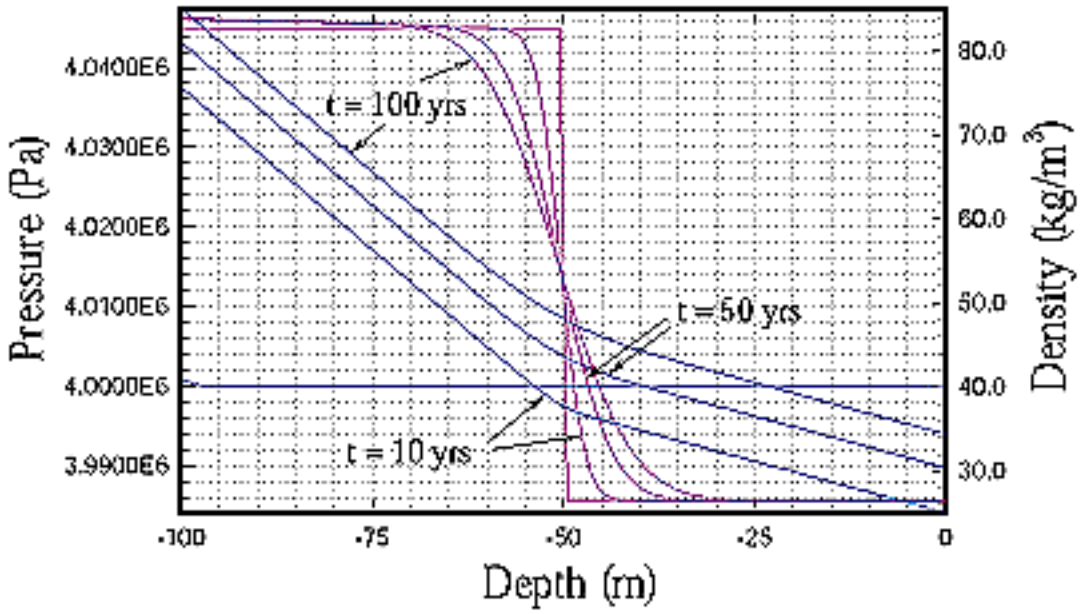


Figure 4. Profiles of pressure and gas density at t = 0, 10, 50, and 100 years during gravity-stable diffusive mixing in the system H2O-$CO_2$-$CH_4$.

*Work Next Quarter*: Diffusive and advective mixing studies will be carried out using both ADM and DGM. Further CSEGR simulations will be completed in preparation of a paper on the topic. Discussions of potential CSEGR pilot sites will continue and be expanded to include possible use of acid gas injection projects.

**Subtask A-3: Evaluation of the impact of $CO_2$ aqueous fluid and reservoir rock interactions on the geologic sequestration of $CO_2$, with special emphasis on economic implications.**

**Accomplishments:**

- Reaction-progress-chemical thermodynamic calculations show that clays may be an important component in the possible suite of secondary minerals that may form during a $CO_2$ injection process. Clays can have an important impact on transport processes which needs to be evaluated by reactive chemical transport modeling.

**Summary:**

Numerical simulations are being carried out to evaluate geochemical changes accompanying injection of a waste stream containing $SO_2$, $NO_2$, and $H_2S$. Simulations are equivalent to batch-type (closed system) reactions, including full-dissolution kinetics (e.g., acid catalysis) for all of the mineral phases present in the reservoir rock. A rock composition is used with modal abundances appropriate for a feldspathic-sandstone reservoir (containing clay and carbonate with and without a Fe-bearing phase), and a carbonate reservoir (comprised of calcite, dolomite, and siderite).

The impact of $SO_2$ was shown in calculations of the total number of moles of C in the fluid under several equilibrating gas-phase compositions: 80 b $CO_2$, 80b $CO_2$ and 10 b $H_2S$, and 80 b $CO_2$ and $10^{-6}$ b $SO_2$. Although the same sequestering processes are occurring in each of the 3 runs, the results are dramatically different in the case of $SO_2$. Even though the net amount of $CO_2$ sequestered as the mineral dawsonite after 500 years increases when the acid gases are added (0.400 moles with $CO_2$, 0.401 moles with $CO_2$, & $H_2S$, and 0.437 moles with $CO_2$ and $SO_2$), the amount of $CO_2$ remaining in solution after 500 years is essentially equal to the starting amount when $SO_2$ is present. This results from the dissolution of nearly all the calcite initially in the rock as the sulfuric acid is neutralized. The pH of the fluid, after the initial equilibration with the gas phase in the absence of rock, is 3.01 ($CO_2$), 2.98 (for $CO_2$ and $H_2S$), and 0.4 (for $CO_2$ and $SO_2$). Because $H_2S$ is a much weaker acid than $H_2SO_4$, it dissolves only a trivial additional amount of the calcite (beyond that due to $CO_2$ alone).

*Progress This Quarter*: This quarter simulations were carried out of the reaction of a NaCl brine that was initially equilibrated with a gas phase consisting of 80 b $CO_2$ and $10^{-2}$ b $NO_2$ this then allowed to react with the feldspathic sandstone reservoir in isolation from the gas phase at 60°C. This low $NO_2$ fugacity, when equilibrated with water, is sufficient to drive the pH to a low value (pH = 1.0), because it is readily converted to the strong acid $HNO_3$. Because the N-O bond is relatively strong, there is a kinetic inhibition of the equilibrium between aqueous species such as $NO_2^-$ (and $NO_3^-$) and $N_2$ species, such as $N_2$(aq). In this simulation we have assumed that in the short-term redox disequilibria will pertain, so we have set the initial $fO_2$ to a value high enough ($10^{-20}$) to make $NO_3^-$ the stable aqueous species and we have suppressed $N_2$(g) and $N_2$(aq). None of the gas fugacities have been fixed, however, so both $O_2$(g) and $CO_2$(g) may evolve as the calculation proceeds. The results during 30 years of reaction are presented in Fig. 5.

Notice that in this simulation (Fig. 5) the reservoir rock carbonate minerals (calcite and siderite) react rather quickly with the dissolved $CO_2$, raising the pH until the calcite is essentially equilibrated with the resulting solution. The siderite over this same period is completely reacted away, owing to the specified initial $fO_2$ condition, because the high $O_2$ fugacity makes hematite thermodynamically stable relative to siderite, even at the high $CO_2$ fugacity. The existing carbonate minerals are not sequestering the waste stream $CO_2$ in this case; indeed, they are adding $CO_2$ to the system. Because it is a closed system calculation, the $CO_2$ fugacity rises from the initial 80 b to 108 b, and so $CO_2$(aq) rises from 1.32 to 1.77 m, as 17% of the calcite and essentially all of the siderite dissolves over a 2-month period. The pH at this point has risen to 4.60 from the initial 1.0 value. The only form of sequestration at this point is the $CO_2$ present in dissolved form in solution. Another interesting consequence of the destabilization of the siderite owing to the high $fO_2$ in this simulation is that it supplies $Fe^{3+}$ to solution, which can react with the $Al^{3+}$ and $SiO_2$(aq) being supplied from K-feldspar dissolution, as well as $Ca^{2+}$ from calcite to form both Ca- and K-nontronite clays. These clays become the primary silica sink.

From this point forward in the calculation the principal reaction involves dissolution of the K-feldspar at the still slightly acid pH. However, the Al released from the K-feldspar combines with Na from the brine and dissolved $CO_2$ to form the mixed hydroxycarbonate mineral dawsonite. This new secondary mineral is sequestering $CO_2$ via mineral trapping. Dawsonite becomes the primary sink for Ca and the Ca-nontronite clay becomes unstable relative to it. The silica released from the dissolving K-feldspar and Ca-nontronite is precipitated as the K-nontronite clay, as well as going into growth of additional quartz and some minor chalcedony. Relatively soon thereafter, the SiO2(aq) concentration decreases to the point that chalcedony is no longer stable and only K-nontronite remains as a stable silica sink. The chalcedony that formed is completely dissolved away. Notice that the absolute abundance of quartz is so much larger than the other minerals that we have not plotted it. It grows in linearly at a rate determined by its kinetic rate law, increasing in volume from 1804 $cm^3$ to 1807 $cm^3$ after 30 years. The K-nontronite and dawsonite both grow in at a rate determined by the dissolution rate of the K-feldspar.

Although the appearance of Fe-bearing clays in this simulation is a direct consequence of the specified initial $fO_2$(g) conditions, it does point out that clays may be an important component in the possible suite of secondary minerals that may form during a $CO_2$ injection process. They can have an important impact on transport processes. This effect will need to be evaluated using reactive transport modeling that couple chemistry and hydrology.

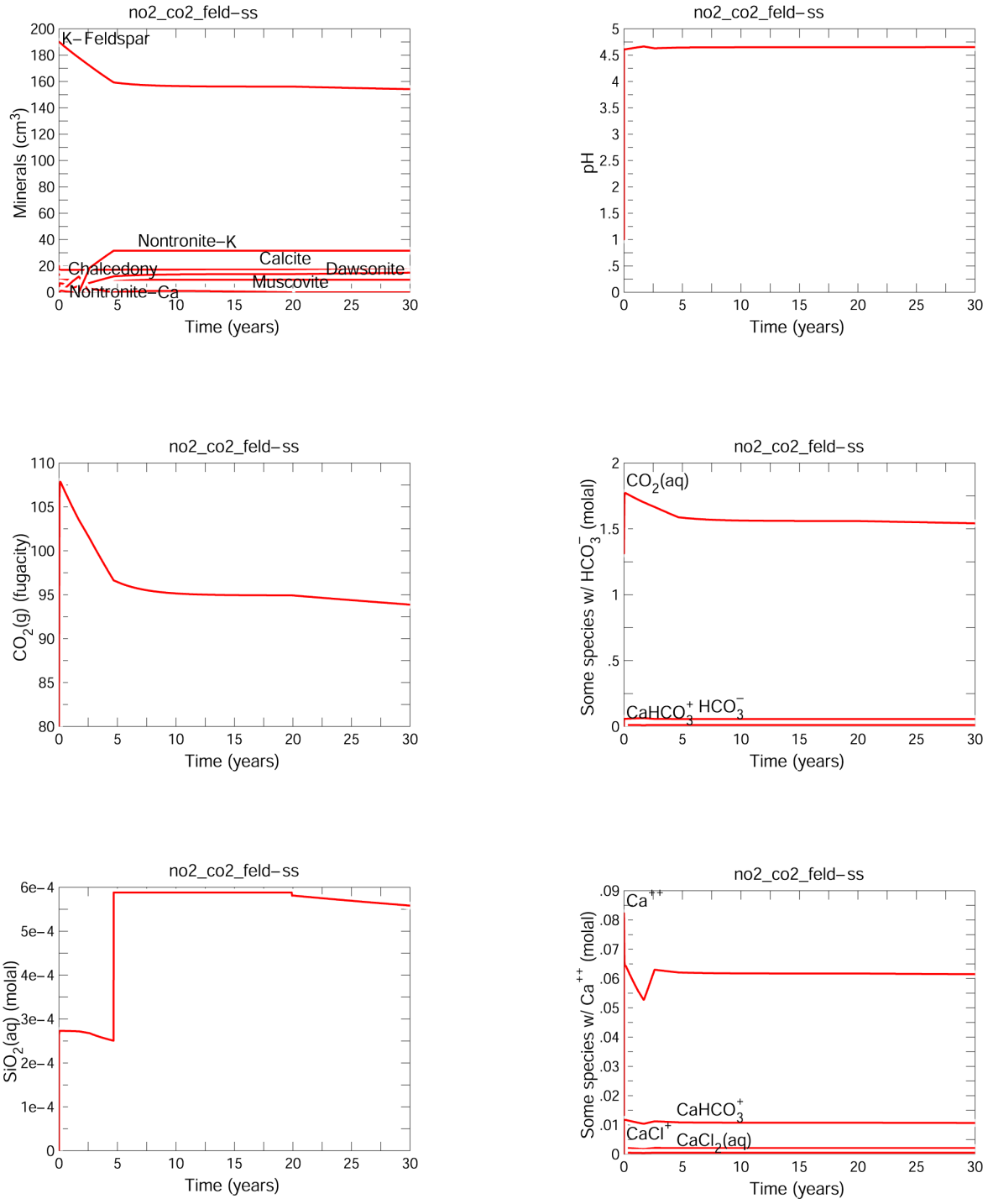


Fig. 5

*Work Next Quarter*: Investigation of the impact of other contaminants ($SO_2$, $H_2S$, $NO_2$, etc.) in the $CO_2$ waste stream will continue. The plan is to next begin the process of accounting for the impact of fluid flow on sequestration by conducting open system (reactive transport) calculations analogous to the closed system calculations made to date. The code CRUNCH (Steefel, 2001) will be used to make 1d calculations with full chemistry equivalent to all the previous runs. Initiation of the reactive transport calculations was delayed for a quarter because a computer purchased for the purpose was faulty. The manufacturer is replacing the machine.

## Task B: Evaluate and Demonstrate Monitoring Technologies

**Subtask B-1: Sensitivity modeling and optimization of geophysical monitoring technologies**

**Accomplishments:**
- Reservoir simulation has been combined with geophysical simulation, field measurements, and data analysis to illustrate the application of crosswell seismic and electromagnetic techniques for monitoring $CO_2$ injection in the Lost Hills, California oil field.
- Injection of $CO_2$ produced changes in electrical conductivity and seismic velocity which were spatially correlated with the location of a mapped fault.

**Summary:**
The objectives of this task are to: (1) demonstrate methodologies for and carry out an assessment of the effectiveness of candidate geophysical monitoring techniques, (2) provide and demonstrate a methodology for designing an optimum monitoring system, and (3) provide and demonstrate methodologies for interpreting geophysical and reservoir data, to obtain high-resolution reservoir images.

The Chevron $CO_2$ pilot at Lost Hills, California, is being used as an initial test case for developing these methodologies (see Subtask B-2 for background information). Work to date has focused on modeling the geophysical response of seismic and electromagnetic (EM) surveys made before and after injection of $CO_2$. The first step in this process was to perform a reservoir simulation (provided by Chevron) of fluid production (oil, water, gas) and fluid injection (water flooding) that took place before and after $CO_2$ injection. The reservoir model simulations provide estimates of porosity, fluid saturation, pressure, and distribution as a function of lithology in the reservoir. Using well logs and rock physics models, we converted this information to seismic velocities and electrical conductivity. Forward simulations were then performed to generate the seismic wavefield that would be sampled by a crosswell seismic survey and the electrical field that would be sampled by a crosswell EM survey. The numerical geophysical data generated from these time snapshots were then processed through seismic tomographic and EM inversion routines to produce images of time-lapse changes in electrical conductivity and seismic velocity (for comparison with the changes produced in the flow simulator).

The results established that geophysical data has the potential to accurately map changes in the reservoir on a scale greater than the fractures themselves and provided confidence that geophysical imaging could predict changes in the reservoir, provided that a good model is available to link geophysical parameters to reservoir parameters.

*Progress this Quarter*: Work during this quarter focused on analysis and interpretation of the crosswell seismic and EM measurements. The baseline EM and seismic surveys were conducted at the same time. There were two EM surveys conducted. One operated at 800 Hz and covered most of the depth interval from 1400 to 2100 feet; the second survey operated at 4000Hz and covered only the depth interval 1600 to 1850ft. The repeat surveys were all separated in time. The first repeat EM survey was conducted in April 2001 with the 4000Hz system. The repeat seismic survey was conducted in May 2001 and the final EM survey was conducted with the 800 Hz systems in July 2001.

The EM data sets were inverted to produce a cross section of electrical conductivity by assuming a conductivity structure that was constant in the direction normal to the imaging plane, Newman (1995). The seismic data was inverted using a proprietary algorithm developed by TomoSeis Inc. that parameterized the model in terms of layers interpolated between the wells where each layer can have laterally varying horizontal velocity. The crosswell images of electrical conductivity and seismic velocity were differenced to form images of time-lapse changes in conductivity and velocity. These are shown in Figure 6. A red to blue color scale is used where blues are negative changes and reds are positive changes. Blue zones correspond to zones where the conductivity or velocity decreased with time. All three images in Figure 6 use the same magnitudes on the color scale. The location of a fault mapped in wells OBC1, 11-8WR and OBC2 is shown as a red line. The expected location of the hydraulic fracture used for water injection is shown as a blue line and the expected location of the hydraulic fracture used for CO2 injection is shown as a green line. The actual locations where the 11-8WR well was perforated for fracturing are shown by the magenta dots on top of the green line.

First consider the changes in electrical conductivity between September 2000 and April 2001 (left panel Figure 6). On either side of the image are areas where the conductivity has increased (red) as was seen in the repeat resistivity logs taken in January 2001. In these areas the conductivity has increased beyond the January values. The center portion of the April-Sept difference image shows a decrease in conductivity. The location of this zone of decrease is shifted towards OB-C1 from the expected fracture locations, but it must be noted that these expected fracture locations are only estimates based on regional stress field and the actual locations could be quite different. In addition the fracturing of the reservoir is most likely more complicated that a single vertical crack.

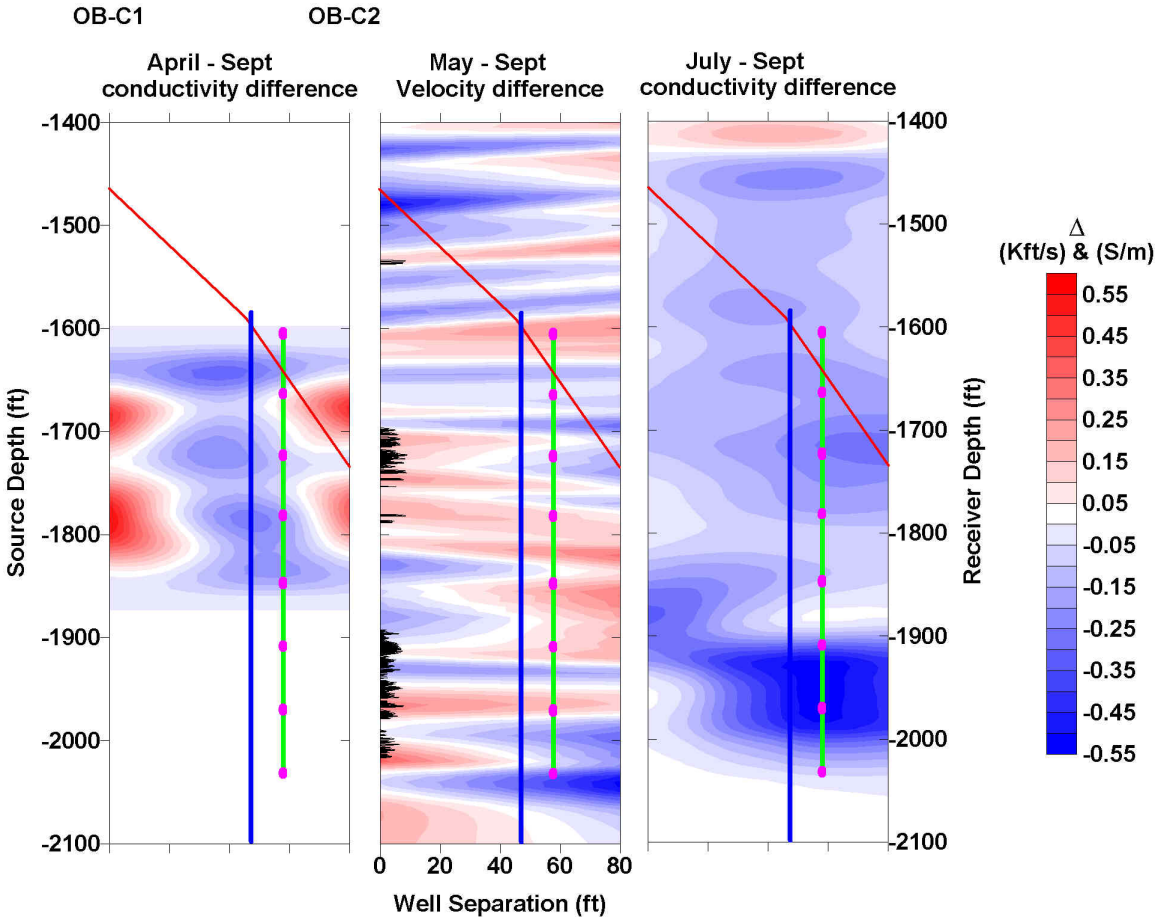


**Figure 6** *Time-lapse changes in electrical conductivity and seismic velocity during $CO_2$ injection. Left panel: conductivity change between April 2001 and September 2000. Middle panel: velocity change between May 2001 and September 2000. Black log on left is gas saturation measured in September 2000 with a maximum of 0.15 percent. Right panel: conductivity change between July 2001 and September 2000. Red line is mapped fault seen in OB-C1, 11-8WR (20 feet behind the image plane) and OB-C2. Blue line is expected fracture used for water injection prior to September 2000. Green line is expected fracture used for CO2 injection after September 2000.*

It is interesting to note that the zone of decrease in conductivity is orientated sub-parallel to the mapped fault implying propagation of fluids in a zone that is aligned with local faulting.

The velocity changes shown in the middle panel of Figure 6 have much higher spatial resolution than the conductivity change images due to the velocity layering of the starting model and the differences in the model regularizations used between the EM and seismic inversions. In general the velocity changes have a more layered appearance with the exception of the zone between 1700 and 1900 ft depth that shows a zone of increased velocity that is orientated parallel to the fault. The gas saturation log observed in

OB-C1 prior to $CO_2$ injection is overlaid on the velocity changes and will be discussed later when we interpret the changes in terms of the rock properties model.

The changes in electrical conductivity between July 2001 and September 2000 are shown in the far right panel of Figure 6 and show considerable change from the earlier conductivity difference image. All of the initial increase in conductivity caused by an early influx of water has gone. Only negative to zero changes in conductivity remain. In addition the zone of change as moved toward the OB-C2 well and is located along the mapped fault. The largest decrease in conductivity occurs between 1900 and 2000 ft depth centered on the expected fracture location for $CO_2$ injection. The zone between 1700 and 1900 ft depth of increased velocity correlates with a zone of little change in conductivity in the July-September image.

The rock properties model developed by multi-parameter regression fitting to observed log data can be used to link changes in geophysical parameters to changes in reservoir parameters. To do this we have used the results of the reservoir flow simulations to estimate the reservoir pressures at the start of $CO_2$ injection as well as the change in pressure that is expected as the $CO_2$ injection proceeds. These numbers should be reasonably close to the true values since we know the down hole pressures at the injectors and producers and because the pressure response is in general a very smooth function not strongly influenced by small local inhomogeneities.

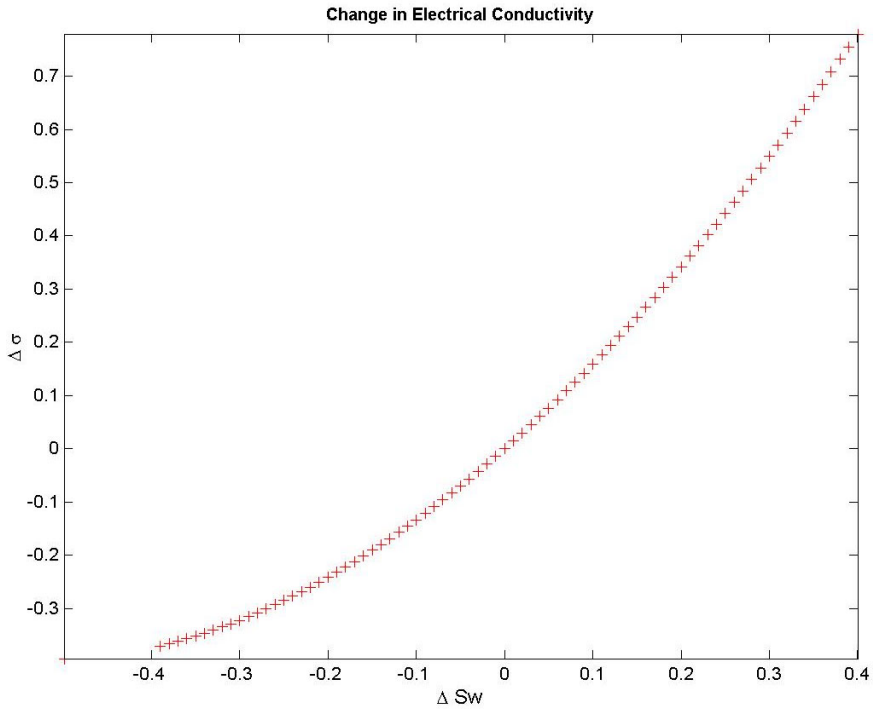


**Figure 7** *Change in electrical conductivity versus change in water saturation ($S_w$) for the Archie's Law model derived from well log data.*

The electrical conductivity is a much simpler function of reservoir parameters than is the velocity. Using Archie's law (Archie 1942) and assuming that the porosity remains unchanged means that electrical conductivity changes will only occur if the water saturation or the pore fluid water conductivity change. In this application where water flood has been in effect for over 6 years we assume that the pore fluid water has reached equilibrium between injected and native water and thus as $CO_2$ injection moves fluids the pore water does not change. This allows us to interpret conductivity changes solely in terms of water saturation changes. Figure 7 shows the change in electrical conductivity as a function of the change in water saturation for the well log derived model using the average water saturation prior to CO2 injection (0.5) as a reference. In the zone where $S_w$ changes between 0 and –0.2 the relation is almost linear with a slope of 1, so that a change in electrical conductivity of –0.1 corresponds to a change of –0.1 in $S_w$.

Using the time-lapse changes in electrical conductivity (Figure 6) and the model (Figure 7) we can estimate the time-lapse changes in water saturation.

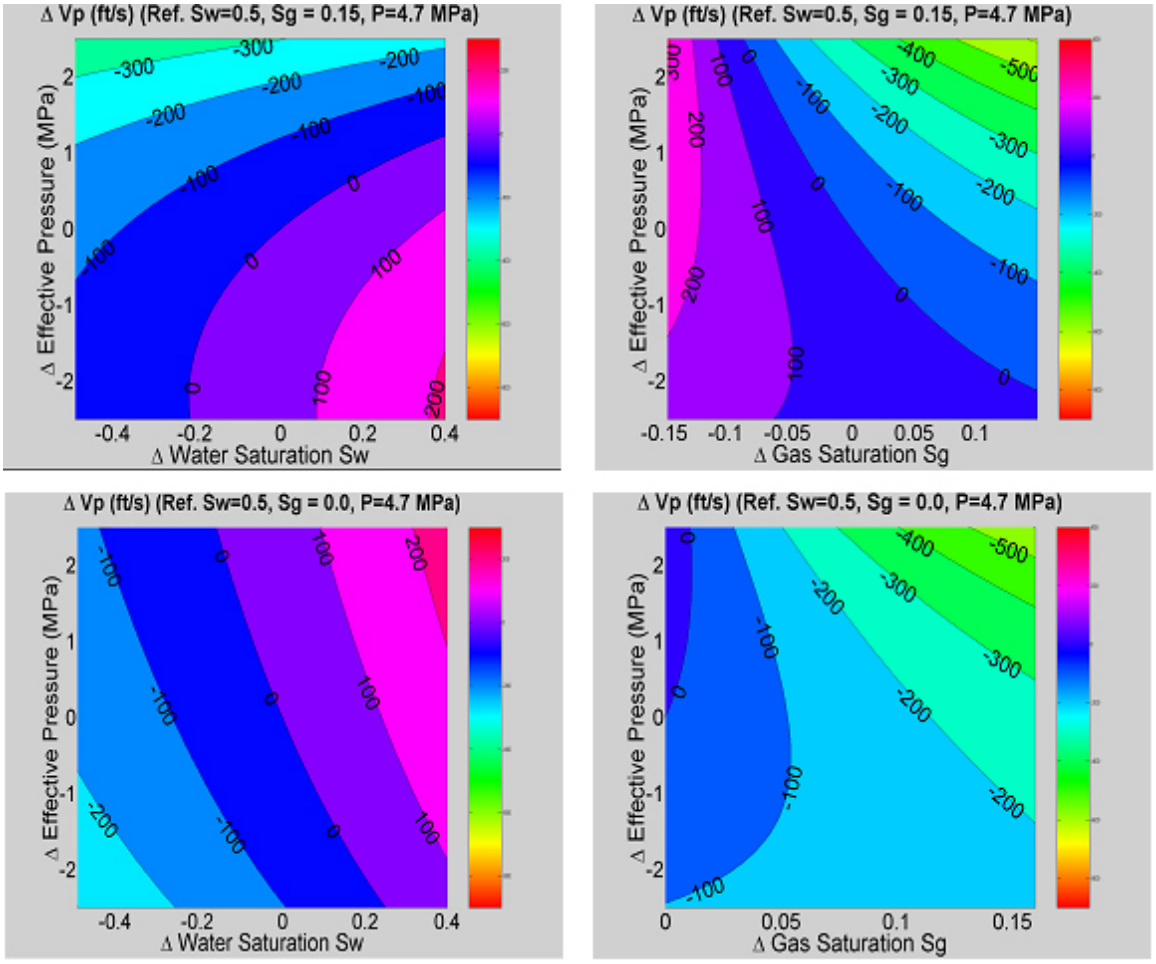


**Figure 8** *Contours of changes in velocity. The reference effective pressure is 4.7 MPa and the reference water saturation is 0.5.*

The velocity of the formation is a function of several parameters, the most important of which are effective pressure (the difference between lithostatic and pore pressure), water saturation and gas saturation. Since we can only visualize changes on two-dimensional contour plots we will consider two cases when interpreting the velocity changes, with and without native gas in the formation. The presence of gas in the formation drastically changes how the velocity behaves as a function of pressure and water saturation. We have done these calculations for methane as well as $CO_2$ with the $CO_2$ behaving very similarly to the methane. So for our discussions here we will use the word gas to mean either methane or $CO_2$ in the gaseous state.

The flow simulation models have shown that the effective pressure would be near 4.7 MPa at the end of water flood in September 2000 and that the $CO_2$ injection would increase the pore pressure, and thus decrease the effective pressure, by about 1.5 MPa. Figure 8 shows the change in velocity about a reference model that represents conditions at the beginning of $CO_2$ injection. The top two panels are for an initial gas saturation of 0.15, an average value observed in near by wells. The bottom two panels are for a case with no gas present.

From the time-lapse changes in conductivity we estimate a water saturation change between –0.1 and –0.2 in the central portion of our image plane. From the flow simulations we have a change in effective

pressure of approximately –1.5 MPa. These two values give values of velocity change from the contour plots in Figure 8. In the case where gas is present (upper left panel) the changes in $S_w$ and pressure produce a small positive (-0.1 Sw) or a zero (–0.2 Sw) change in velocity. If gas saturation is decreased by 0.1 to 0.15 by dissolution into the oil as the pore pressure increases (upper right panel) the velocity increases by 150 to 200 ft/s.

In the parts of the formation where no gas is present to begin with a change in pressure of –1.5 MPa and a change in water saturation of –0.1 produces a decrease in velocity of –100 ft/s. When gas is added (lower right panel Figure 8) an increase of 0.05 in the gas saturation decreases the velocity by –100ft/s.

We interpret the time-lapse electrical conductivity images to mean that the water saturation has decreased by approximately –0.2 in the zones of maximum change. This could be due to either and increase in oil saturation or an increase in gas ($CO_2$) saturation or some combination of the two. The changes in velocity between 1500 and 2000 ft depths are +- 150 ft/s. A decrease of –150 ft/s in the zones without native gas can be explained solely on the basis of the change in water saturation and effective pressure without any $CO_2$ being introduced. An increase in $CO_2$ saturation of 0.05 in addition to the pressure and water saturation change effects would produce velocity decreases on the order of –250 ft/s. These magnitude decreases are only seen at the upper part of the image on the left side between 1400 and 1500 ft depth and on the lower right side of the image between 2000 and 2100 ft depth.

The areas of the velocity change image (center panel Figure 6) that show an increase in velocity correlate with regions were gas was present at the beginning of $CO_2$ injection. The exception is the layer just below 1600 ft that increases in velocity but where no gas was logged. Time-lapse increases in velocity of the same magnitude have been observed in other parts of the Lost Hills field and are associated with gas dissolving in oil due to the increase in pore pressure associated with injection. In addition the rock properties model predicts the increase of 100 to 200 ft/s for a decrease of 0.1 to 0.15 in gas saturation. This leads us to interpret the areas of increased velocity as areas where native gas has been driven into solution by pressure increases.

The final time-lapse image is the change in conductivity between July 2001 and September 2000 (right panel Figure 6). It appears that by July the major changes have moved toward the OB-C2 well and are not aligned with the mapped fault. The zone of positive velocity increase between 1700 and 1900 ft (pressure effects on gas only) correlates with a zone of minimal change in the conductivity image. There is a zone of large change (-0.4) in conductivity centered on the expected $CO_2$ fracture location in the depth interval 1900 to 2000 ft. The largest velocity decrease is at a depth of 2050 ft on the same side of the image. We interpret these decreases in velocity and conductivity over what is seen in other parts of the image as indicating the presence of $CO_2$.

*Work Next Quarter:* The flow simulation model will be refined both in terms of modified permeabilities (as inferred from the geophysical imaging) and incorporating small-scale faulting (as seen in the logs). The flow simulations will be updated to more closely match the observed changes. Once a flow simulation model is derived with improved predictive capabilities, the pressures from this model will be used as illustrated above to convert the difference images into images of change in water saturation and $CO_2$ saturation. Finally, a single-well seismic-reflection data set is being analyzed in attempt to directly image the fracture location and estimate the fluid saturations within the fracture itself. If this is successful, this information will be incorporated into our EM and seismic inversions to further refine these images

**Subtask B-2: Field data acquisition for $CO_2$ monitoring using geophysical methods**

**Accomplishments:**

- Processing of the single well seismic survey conducted after $CO_2$ injection at the Lost Hills field produced a reflection image corresponding to the gas filled hydrofracture.
- Design was completed of field surveys to obtain coarse point electrode and casing electrical resistance tomography (ERT) surveys in conjunction with crosswell EM surveys at the Vacuum Field $CO_2$ EOR project.

**Summary:**
The goal of this subtask is to demonstrate (through field testing) the applicability of single-well, crosswell, surface-to-borehole seismic, crosswell electromagnetic (EM), and electrical-resistance tomography (ERT) methods for subsurface imaging of $CO_2$.

The $CO_2$ injection pilot operated by Chevron USA in Lost Hills, California, provides an early opportunity to test several of these techniques. This pilot is divided into four injection-centered, 2.5-acre patterns as shown in Figure 10. The figure also provides some interpreted geology for the site. The production interval is from 1,200 ft to 2,100 ft below ground surface, and the $CO_2$ injection interval is from 1,500 ft to 2,000 ft. The $CO_2$ injection began in August 2000 at a relatively low flow rate of 125 million cubic feet (Mcf) per day and was gradually increased to 425 Mcf/day per injection well. The injection pressure is being held at 800–900 psi and the reservoir temperature is about 100° F. At these pressure and temperature conditions, the $CO_2$ is expected to be in gas phase. In early January 2001, $CO_2$ injection was stopped in the four injection wells because of sanding problems in some of the producing wells. The wells were cleaned out, and $CO_2$ injection has been restarted in one of the injection wells.

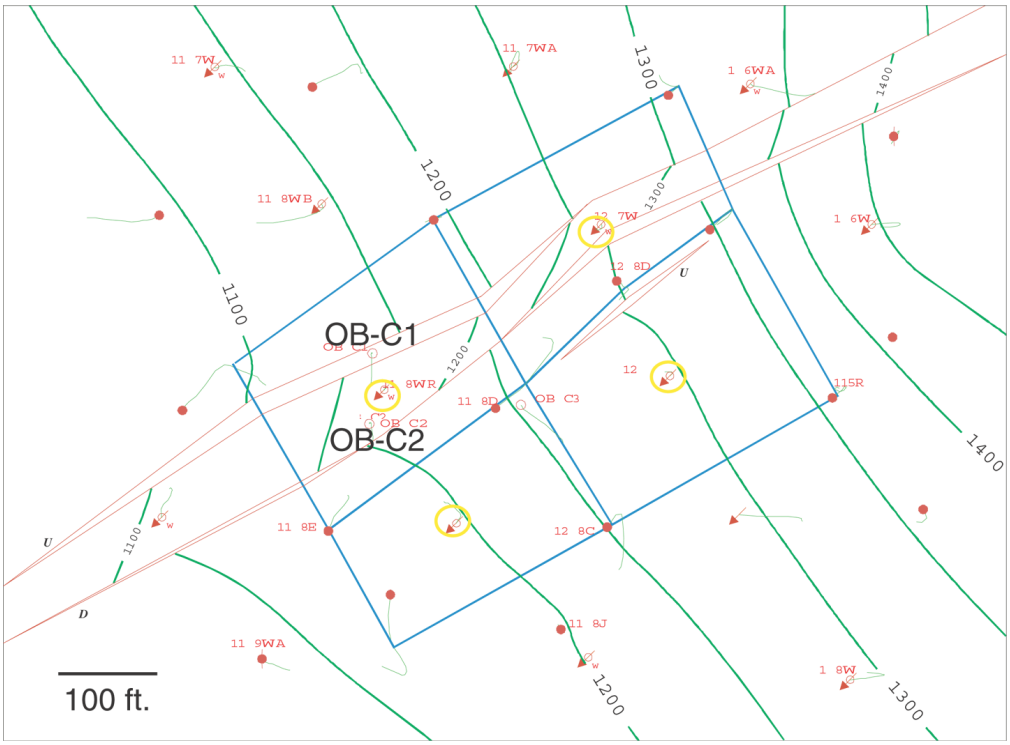


Figure 9. *$CO_2$ injection site (blue lines) with contoured top of reservoir (green lines) and interpreted faults (red lines).*

The reservoir volume around injection well 11-8WR has been monitored by high-resolution geophysical techniques. Pre-injection crosswell seismic and EM measurements were made between observation wells OB-C1 and OB-C2, and single-well seismic measurements were made in OB-C1.

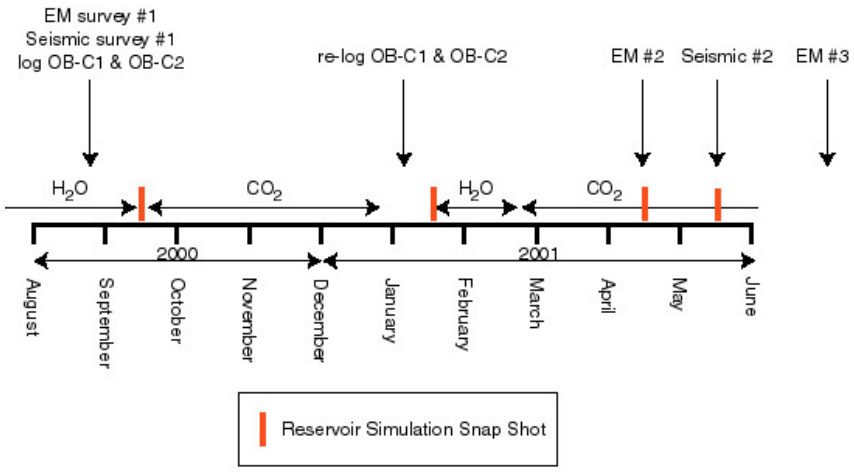


Figure 10. *$CO_2$ injection experiment time line (also showing times of reservoir simulations used in Subtask B-1).*

The second EM survey was conducted in mid-April 2001, and the second seismic survey was conducted in May 2001. A third EM survey was carried out in July. This third EM survey will bracket the second seismic survey and provide a means to interpolate the conductivity changes to the same time as the seismic changes. The data from these surveys are the basis for a joint seismic-electromagnetic inversion to constrain reservoir models of $CO_2$ distribution (as discussed in Subtask B-1).

In a parallel activity, a field program to evaluate electrical/electromagnetic methods for monitoring $CO_2$ injection was developed. Through interactions with Texaco and EMI (a commercial EM survey company), a joint field program has been developed that will permit both crosswell EM and ERT surveys to be obtained during a $CO_2$ flood designed for EOR. The location of this project is Texaco's Vacuum Field in New Mexico. Infill drilling has been conducted, so that the initial 40-acre spacing has been reduced to 10 acre 5-spots. This presents a poor aspect ratio for high-resolution imaging, but will permit realistic conditions for testing the sensitivity of the methods. Texaco is making available both open and cased holes in the target area, so that both an ERT point-electrode crosswell survey and a casing survey are planned (see Figure 11). The coarse-spaced point-electrode crosswell study will permit validation of the range of resistivity changes observed over the operational depth interval and permit direct comparison with EMI's crosshole EM surveys.

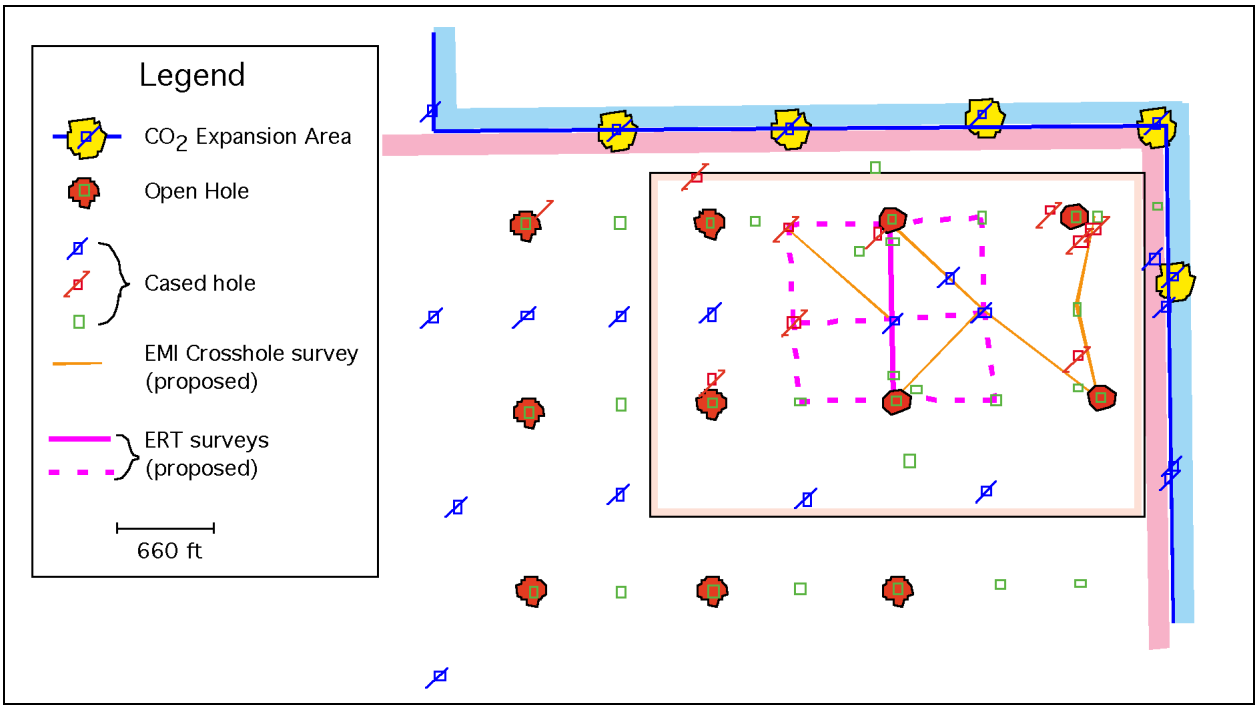


Figure 11. *$CO_2$ expansion project and proposed surveys in Texaco Vacuum Field.*

*Progress this Quarter:* As previously reported, at the Lost Hills site a single well seismic data set was acquired in addition to the crosswell measurements. The survey was conducted with a piezoelective source and hydrophone sensors. Data from the pre- and post-injection surveys in well OB-C1 are shown in Figure 12. This quarter the data from the post injection survey was processed to produce the reflection. Image shown in Figure 13. The image shows a strong event about 35 feet from the well, and a second weaker event about 50 feet from the well. These distances correspond to the perpendicular distances from the well to planes of hydrofractures generated in neighboring wells. The depth of the image in the well also corresponds to the depth of the perforation intervals for the hydrofractures. The interpretation is that the event is the reflection from the $CO_2$-filled hydrofractures.

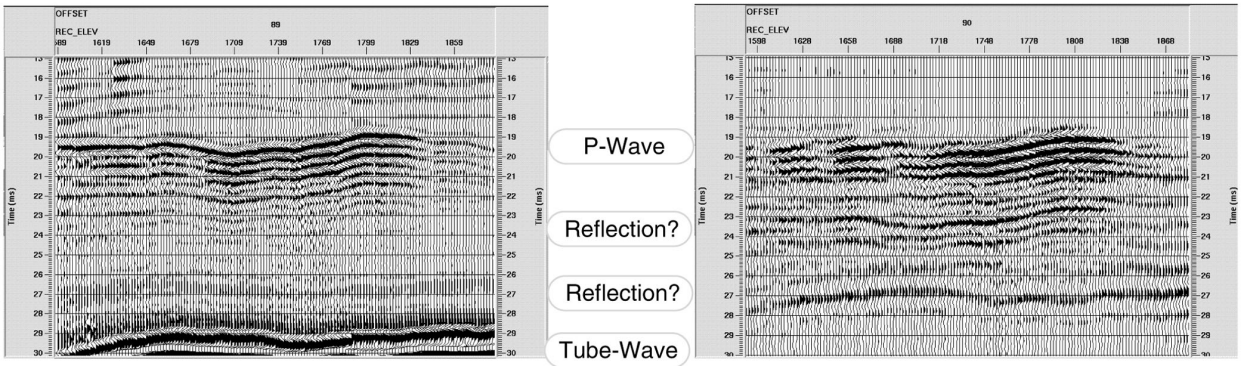


Figure 12. *Single-well data from OB-CI pre-injection (left) and post-injection (right).*

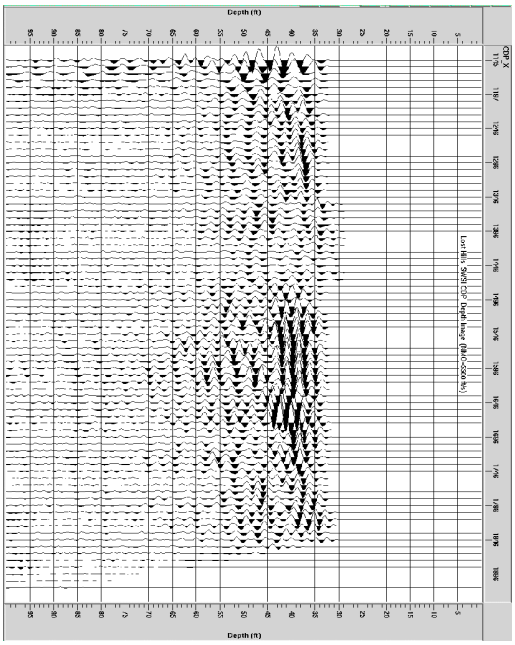

Figure 13 *Processed post-injection single well image from well OB-C1.*

In the studies evaluating electrical/electromagnetic methods for $CO_2$ monitoring in the Vacuum Field, the primary activity this quarter was design of the field program. Workplans were developed to obtain baseline (pre-injection) surveys originally scheduled for August or September. The unexpected opportunity to access uncased wells in the field will permit a crosswell point electrode survey to be obtained. A point electrode string suitable for logging the partially uncased wells was designed and two were constructed. These instrumentation strings will connect to conventional wireline logging cable, permitting standard logging equipment to be used for the field program. In the target area, the two wells that are open (lacking casing) in the target interval required modification to enable us to access them for a casing survey. To address this issue, instrumentation was designed and constructed, consisting of a weighted steel cable that will be lowered into each of these wells, simulating the presence of casing to the bottom of each well.

*Work Next Quarter*: Work will continue in processing and analyzing the post-injection seismic surveys, including processing of the orbital vibrator data sets. These results will be integrated into the joint inversion and reservoir model. At the Vacuum Field, initial baseline surveys will be performed. Subsequent "time-lapse" surveys would be fielded after sufficient time has elapsed to detect significant changes in the reservoir.

**Subtask B-3: Application of natural and introduced tracers for optimizing value-added sequestration technologies**

**Accomplishments:**

- The pressure dependence of stable carbon and oxygen isotope partitioning between $CO_2$ and representative geological materials varies little over the pressure range tested, but does depend on whether the solid contains hydrocarbons.
- Preliminary $CO_2$ adsorption-desorption measurements have been made on a select suite of carbon materials as a prelude to similar measurements to be conducted on geological reservoir materials used in isotope partitioning experiments.

**Summary:**

The overall goal of this effort is to provide methods that utilize the power of natural and introduced tracers to decipher the fate and transport of $CO_2$ injected into the subsurface. The resulting data will be used to

calibrate and validate predictive models used for (1) estimating $CO_2$ residence time, reservoir storage capacity, and storage mechanisms; (2) testing injection scenarios for process optimization; and (3) assessing the potential leakage of $CO_2$ from the reservoir.

To date, work has focused primarily on isotopic tracers. Effort has been directed to accessing carbon and oxygen isotope change as the $CO_2$ reacts with potential reservoir phases. Both laboratory isotope-partitioning experiments and mass-balance isotopic-reaction calculations have been performed. In addition to investigation of generic rock fluid systems, studies specifically focused on the Chevron Lost Hills $CO_2$ pilot have also been carried out.

Results show that temperature dependence of stable carbon and oxygen isotope portioning between $CO_2$ and representative geological materials can vary considerably, depending on whether the solid contains hydrocarbons. In addition, mass-balance isotopic-reaction calculations indicate that the magnitude and trajectory of change of carbon and oxygen isotopes in $CO_2$ reacted in the system calcite-$CO_2$-$H_2O$ can vary markedly, depending on the initial isotopic compositions of the $CO_2$, $H_2O$, and $CaCo_3$, the temperature of interaction, and the relative abundance of each constituent.

*Progress this Quarter*: Efforts this quarter have focused on two interrelated activities: (a) investigation of the pressure dependence of C and O isotope partitioning between $CO_2$ and select geological materials (e.g., quartz, calcite, montmorillonite, Lost Hills core), and (b) detailed measurements of $CO_2$ adsorption-desorption on carbon materials.

Carbon and oxygen isotope partitioning experiments in static systems have been conducted at a temperature of 20$^{o}$C as a function of $CO_2$ pressure which was varied from less than 0.01 bar to 0.1 bar. As with our previous studies, both C and O isotope values of the free $CO_2$ are always enriched in the heavier isotope ($^{13}C$ or $^{18}O$) relative to $CO_2$ adsorbed onto mineral surfaces. The overall magnitude of the partitioning was generally consistent with what we have reported previously – i.e. the isotopic difference between free $CO_2$ and sorbed $CO_2$ increased, in order, from quartz to calcite to Lost Hills core, and finally to montmorillonite for carbon, and from quartz to calcite to montmorillonite to Lost Hills core for oxygen. The effect of pressure increase is much less pronounced compared to the magnitude we observed for the temperature effect. For crystalline phases such as quartz, calcite and montmorillonite, the magnitude of the carbon and oxygen isotope partitioning increased at a rate of only about 0.1 and 0.2 per mil per 20-mbar increases in $PCO_2$, respectively. Isotopic partitioning between $CO_2$ and the Lost Hills core was somewhat greater wherein we observed an increase in carbon isotope partitioning of between 0.2 and 0.3 per mil per 20-mbar increases in $PCO_2$. The change in oxygen was roughly a factor of two greater than carbon for the Lost Hill samples. There is a tendency for the partitioning to reach steady state as pressure approaches 0.1 bar, probably signifying attainment of $CO_2$ saturation on the mineral surfaces.

As a prelude to $CO_2$ adsorption-desorption measurements on our geological materials (e.g. quartz, calcite, montmorillonite, etc.), we obtained a suite of carbon materials that have been used previously in $CO_2$ sorption studies. These include amorphous carbon, graphite, and charcoal. The purpose of this exercise was to test and calibrate our surface area/pore size analyzer for $CO_2$ gas. Our previous experience has only been with the use of either $N_2$ or Kr as adsorbing species. All three-carbon materials exhibit similar sorption isotherm behavior when recast on a per-unit-area-basis. Measurements were conducted at two temperatures: 0 and 20$^{o}$C, the latter being more appropriate for subsurface conditions. The isotherms indicate two distinct regions of coverage that are separated by a wide plateau; this plateau appears broader at 0$^{o}$C. The adsorption at very low pressures (<0.01 torr) is compatible with high-energy adsorption on one array of carbon atoms occupying the prism faces. Additional adsorption at higher pressures then occurs on sites of lesser energy in the more abundant basal planes. The charcoal sample exhibited more of the basal-plane sorption behavior than the other carbon materials tested.

*Work Next Quarter*: Efforts in the next quarter will focus on four main areas:

(a) Write-up the results obtained from the isotope partitioning experiments in static systems for publication.
(b) Initiate $CO_2$ sorption-desorption experiments using Argonne Premium coals as well as Lost Hills core and mineral end-members, quartz, calcite and montmorillonite.

(c) Initiate a modeling effort using Geochemist's Workbench to assess the magnitude of carbon and oxygen isotope partitioning during gas-brine-mineral reactions relevant to subsurface aquifer formation conditions.
(d) Complete construction of flow-through column apparatus and laboratory testing of the applied tracers using the similar geological materials as in the isotopic tracer experiments.

## Task C: Enhance and Compare Simulation Models

**Subtask C-1: Enhancement of numerical simulators for greenhouse gas sequestration in deep, unmineable coal seams.**

**Accomplishments:**
- All candidate numerical codes successfully simulated the first two-benchmark coalbed methane problems.
- Mixed gas adsorption processes are better represented using the extended Langmuir model.

**Summary:**
The goal of this subtask is to improve simulation models for capacity and performance assessment of $CO_2$ sequestration in deep, unmineable coal seams.

Work began with definition of the physical processes that ultimately should be included in coalbed methane (CBM) numerical simulators. Benchmark problems were then developed for testing and comparison of available CBM codes. Problem Set 1 is a single-well test with $CO_2$ injection into a coal seam. Problem Set 2 is an enhanced coalbed methane (ECBM) process with $CO_2$ injection in a 5-spot well pattern. Problem Set 3 is the extension of Problem Set 2 but taking into account the effect of mixed gas diffusion between the coal matrix and the natural fracture system (dual porosity approach). Problem Set 4 is the extension of Problem Set 2 but taking into account the effect of stress on the permeability/porosity of the natural fracture system (Palmer & Mansoori model).

The numerical models being tested are CMG's STARS, CMG's GEM, GeoQuest's ECLIPSE, BP's GCOMP, CSIRO's SIMEDII and ARI's COMET2. Testing of the first two sets of numerical problems has been completed, and website has been established to document the benchmark problems and post solutions. A complementary effort was also initiated to define analytical solutions for multicomponent gas flow in coalbeds coupled with adsorption.

*Progress this Quarter*: A report that compares results (see Figure 14) and describes the current development of the CBM numerical models (see Table) is under preparation. It is found that all numerical models are capable to model the first two sets of simple numerical problems. A conclusion is that it is more appropriate to use an extended Langmuir model to describe the mixed gas adsorption process.

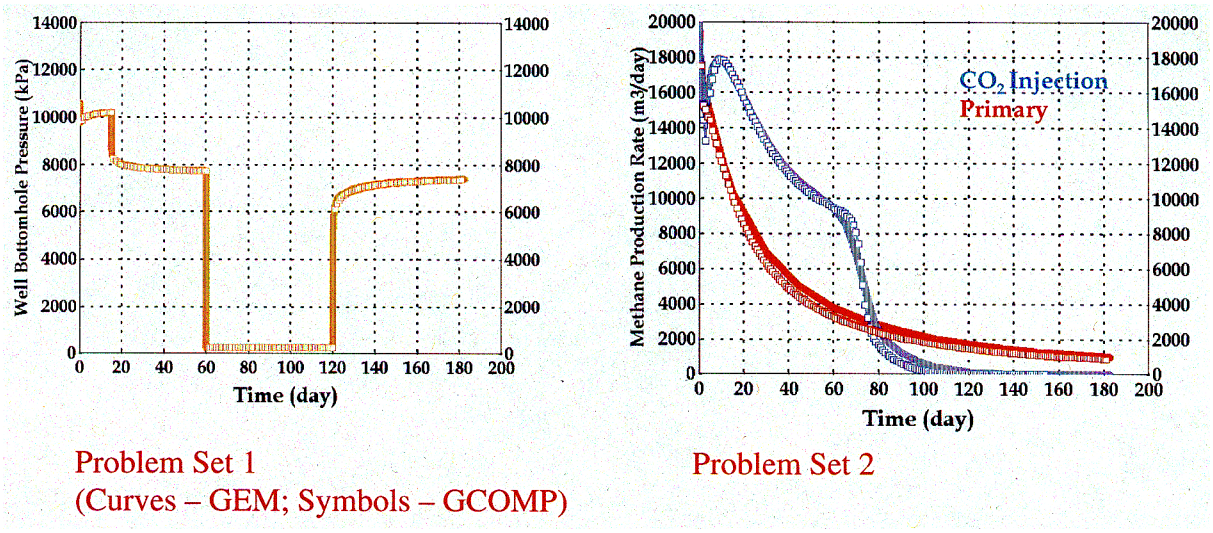


Figure 14

| CBM Simulators | GEM | ECLIPSE | SIMED II | COMET2 | GCOMP |
|---|---|---|---|---|---|
| Multiple Gas Components (3 or more $CH_4$, $CO_2$ & $N_2$) | ✔ | ✘ | ✔ | ✘ | ✔ |
| Dual Porosity Approach | ✔ | ✔ | ✔ | ✔ | ✘ |
| Multiple Gas Diffusion (Different Diffusion Rates) | ✔ | ✔ | ✔ | ✔ | ✘ |
| Multiple Gas Sorption (Extended Langmuir Model) | ✔ | ✘ | ✔ | ✔ | ✔ |
| Stress Dependent Permeability & Porosity | ✘ | ✔ | ✔ | ✔ | ✔ |
| Adsorbed Gas Content Dependent Coal Shrinkage | ✘ | ✘ | ✔ | ✔ | ✔ |
| Adsorbed Gas Content Dependent Coal Swelling | ✘ | ✘ | ✘ | ✔ | ✔ |

Ongoing Development

In other work analytical solutions for multicomponent gas flow in coal beds coupled with adsorption were completed and verified versus finite difference simulation. The system methane, nitrogen, and carbon dioxide were considered as an example. The formulation is completely generic in that the behavior of an injection gas of any composition can be computed.

*Work Next Quarter:* A report on the comparison of the first two problem sets will be completed. Results from problem sets 1 and 2 and new problems sets 3 and 4 will be posted on the ARC website: http://www.arc.ab.ca/extranet/ecbm/ with the new user name: ECBM and password: coal2. Negotiations will continue with Burlington Resources for the release of field data from their $CO_2$-ECBM pilot for a problem set which predicts $N_2$ and $CO_2$ breakthrough.

A report will be prepared detailing the analytical solution method and showing example calculations.

**Subtask C-2: intercomparison of reservoir simulation models for oil, gas, and brine formations**

**Accomplishments:**
- The dates for a first workshop on the code intercomparison project were set for October 29-30 (Monday-Tuesday), 2001, at LBNL. Nine groups from five countries have committed to attending the workshop.

**Summary:**
The objective of this subtask is to stimulate the development of models for predicting, optimizing, and verifying $CO_2$ sequestration in oil, gas, and brine formations. The approach involves: (1) developing a set of benchmark problems, (2) soliciting and obtaining solutions for these problems, (3) holding workshops of industrial, academic, and laboratory researchers, and (4) publishing results.

To date, a set of light benchmark problems have been established. Processes encompassed by these problems include carbon sequestration with enhanced gas recovery, aquifer disposal of $CO_2$ (with geochemical interactions), hydro-mechanical coupled processes, and miscible and inmiscible displacement of oil by $CO_2$. Materials for the intercomparison study have been mailed out, and posted on the Web. A detailed report on study design and milestones as well as specifications for a first set of eight test problems was completed.

*Progress this Quarter*: A scope for a first workshop was developed. It is planned as a working meeting for project participants. The main purpose is to present and review results obtained on the first set of 8 test problems, to discuss and clarify problem specifications as needed, and to develop additional more realistic and comprehensive test problems.

An invitation to attend the workshop was mailed to ten groups in six countries who are participating in the study. Nine groups have confirmed their attendance at the workshop; the tenth group will submit results electronically for presentation at the workshop.

Simulation studies related to the test problems were continued, as were enhancements and revisions in our simulation codes.

*Work Next Quarter:* We will complete simulations of the test problems. We will convene a first workshop in Berkeley that will serve to summarize work done by the different groups to date, as well as charting a course forward to completing the study. Additional more complex test problems will be developed.

## Task D: Improve the Methodology and Information for Capacity Assessment

**Accomplishments:**
- A site was identified in the Houston, Texas area for a field test of $CO_2$ sequestration in a brine formation.
- Preliminary site-specific modeling was performed to assess feasibility and experiment design.

**Summary:**
The objectives of this task are to: (1) improve the methodology and information available for assessing the capacity of oil, gas, brine, and unmineable coal formations; and (2) provide realistic and quantitative data for construction of computer simulations that will provide more reliable sequestration capacity estimates.
As a preliminary step in performing capacity-assessment simulations in brine formations, mathematical models were developed to assess the relative contributions to total sequestration capacity from $CO_2$ (1) in the gas phase, (2) dissolved in the aqueous phase, and (3) in solid minerals. Capacity factors for the three different storage modes were defined as the equivalent gas saturations that would be required to store the same amount of $CO_2$. These capacity factors were partially evaluated through analytical estimates and numerical simulations. As a next step, the effect of formation geometry and heterogeneity has been included in the definition of an updated capacity factor, C given as the product of four factors:

$$C = C_i \bullet C_g \bullet C_h \bullet \phi$$

$C_i$ is intrinsic capacity, which is controlled by multiphase flow and transport phenomena; $C_g$ is the geometric capacity factor, which is controlled by formation geometry; $C_h$ is heterogeneity capacity factor, which is controlled by geologic variability; and $\phi$ is porosity, the fraction of void space within the formation. This formulation was found to be useful for investigating the different processes that influence C and for comparing this approach to that of other authors. In practice, however, one may not be able to separately calculate $C_i$, $C_g$, and $C_h$.

The Texas Gulf Coast was targeted as an area from which a realistic data set could be generated for use in simulation of capacity in brine formations. Location and identifying information were compiled for large industrial $CO_2$ emitters and geologic data for the Frio and Oakville reservoirs were compiled. A realistic scenario for $CO_2$ injection into a brine formation was then designed for a site near Baytown, Texas. The capacity of brine formations for storage of $CO_2$ at the site was assessed using numerical simulation.

*Progress this Quarter:* This quarter another site was selected for a pilot $CO_2$ sequestration experiment in a brine formation. Candidates considered during the past year included six oil-producing reservoirs in West Texas, formerly productive but watered-out zones in the Woodbine of east Texas, potential candidates for secondary recovery in Frio and Miocene reservoirs in the Houston near power plants and refinery $CO_2$ sources. Selection criteria include experiment cost and benefit to the US geologic sequestration program. The Frio Formation in the Houston area was selected because (1) large volumes of $CO_2$ are currently released as a result of power generation and industrial sources in this area and air quality degradation because of the interaction of ambient conditions with industrial concentration is of high concern to the local population, (2) previous work (Hovorka and others, 2000) documented the presence of numerous high-injectivity sandstones that will serve as injection targets and numerous thick shales that will serve as seals, (3) abundant geologic and geotechnical data are available, and (4) infrastructure is well developed, including many inactive wells and easy and low-cost access to needed support for field operations. Little industry experience with $CO_2$ injection into the Frio exists, so one tasks was to provide realistic geologic data, which would be used in numerical simulations to increase understanding of how Frio sandstones are likely to perform for sequestration.

A small company with some acreage in the South Liberty Field, northeast of Houston, has agreed to provide access to three idle wells. One well is proposed for recompletion as a $CO_2$ injector and one or two wells are proposed for recompletion as monitoring wells. The injection target is a brine bearing sand near the top of the Frio. The proposed experiment is designed to test a number of modeling and monitoring technologies. The selected target is in a compartment within a salt dome, and the proposed injection of small $CO_2$ volumes into a volume stratigraphically and structurally isolated from production are important. Other candidates lacking these attributes were rejected because the operator assessed the risk of liability as too high.

Last quarter a probabilistic geologic realization was developed which could be modeled to evaluate the impact of stratigraphic variability on $CO_2$ injection. Generalized but site-specific structural elements were added to determine the feasibility of a proposed experiment. Critical elements include the hydraulic behavior of faults and the dip and structural complexity between the injector and monitor wells. Simulations using realistic permeability, stratigraphic and structural data were used to estimate feasibility and cost of the project. These are summarized in a web document, available at http://www-esd.lbl.gov/GEOSEQ/pilot sims/. Example results are shown in Figure 15 and 16 which show the effect of incorporating heterogeneity in the base model. Specifically, heterogeneity was added to the upper sand and two underlying shaly layers were added to the model to represent the entire Frio B sand thickness of 50 feet (15 m). While the marine flooding shale overlying the upper sand is expected to provide a continuous seal, the fluvial-deltaic shaly layers underlying it are known to consist of lenticular shales intercut by sand channels and splays that may provide pathways for $CO_2$ migration.

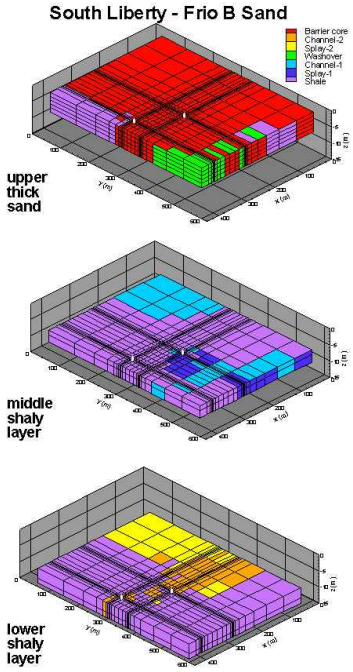


Figure 15

The model consists of nine layers, five for the upper sand (which now includes small amounts of low-permeability shale and intermediate-permeability washover facies) and two each for the underlying shaly layers. Permeabilities and porosities of the different facies are given in the table below.

| Facies | Porosity (%) | Horizontal permeability (md) | Vertical permeability (md) |
|---|---|---|---|
| Barrier core | 32 | 700 | 700 |
| Channel-2 | 30 | 400 | 100 |
| Splay-2 | 30 | 150 | 30 |
| Washover | 29 | 200 | 50 |
| Channel-1 | 30 | 100 | 70 |
| Splay-1 | 28 | 30 | 20 |
| Shale | 10 | 0.001 | 0.0001 |

No appreciable amount of $CO_2$ moves below the upper sand, and the distribution within the upper sand is quite similar to the homogeneous base case. Pressure increases are minimized because brine is able to flow through the sandy facies within the shaly layers.

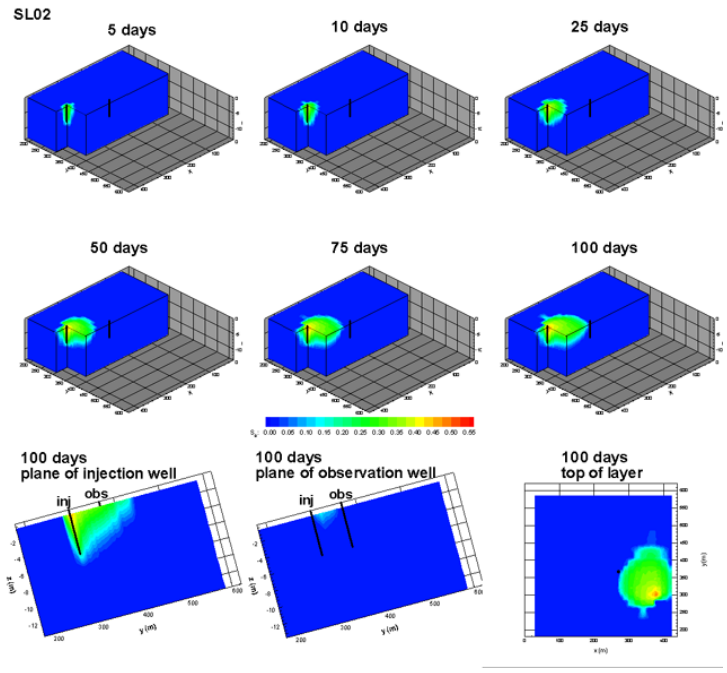


Figure 16

*Work Next Quarter*: We will further experiment with the Frio Formation in the Houston area with models on several scales. Creation of more structural and stratigraphic appropriate input data and initial model runs are goals for next quarter.

**Cost Summary:**

| | **LBNL**<br><br>**(Including subcontract to Stanford, TBEG, and ARC)** | **LLNL** | **ORNL** |
|---|---|---|---|
| **FY01 Funding + carryover** | $857,000 | $371,700 | $377,471 |
| **Quarterly Cost** | $181,500 | $75,000 | $100,147 |
| **FY01 Cumulative Cost** | $535,000 | $271,000 | $254,447 |
| **Remaining Balance** | $322,000 | $100,700 | $123,024 |